PEI/Zr^{4+}-coated Nanopore for Selective and Sensitive Detection of ATP in Combination with Single-Walled Carbon Nanotubes

Siqi Zhang [a,b], Amin Bao [b], Ting Sun [a*], Erkang Wang [b*], Jiahai Wang [a,b*]

[a] College of Science, Northeastern University, Shenyang, 110819, China

[b] State Key Laboratory of Electroanalytical Chemistry, Changchun Institute of Applied Chemistry, Chinese Academy of Science, Changchun, Jilin, 130022, China

*Corresponding author

E-mail: jhwang@ciac.jl.cn; sun1th@163.com; ekwang@ciac.jl.cn;

Tel.: +86-0431-85262334;

Homepage: http://nanopore.weebly.com

Abstract

By virtue of a biomimetic nanopore and single-walled carbon nanotubes, a new sensor for adenosine triphosphate (ATP) detection is designed. As compared to the routine approach, the present scenario does not entail the surface modification of nanopore with analyte-specific probes. The underlying mechanism relies on a symmetric nanopore sequentially modified with polyethyleneimine (PEI) and Zr^{4+} that can quantitate the concentration of ATP-bound aptamer, while other free aptamers are removed by single-walled carbon nanotube (SWNTs). The detection limit of the nanopore sensor is 27.46 nM, and the linear range is from 50 nM to 400 nM. The biosensor with an excellent selectivity against guanosine triphosphate (GTP), uridine triphosphate (UTP), and cytosine triphosphate (CTP) can be applied in the real samples such as Hela cell.

Keywords: nanopore, polyethyleneimine, Zr^{4+}, aptamer, ATP detection, single-walled carbon nanotubes

1. Introduction

In recent years, synthetic nanopores have intrigued scientists in different fields for their easy preparation and functionalization (Ali et al. 2010; Liu et al. 2012). In terms of the bioanalytical applications based on artificial nanopores, many excellent works have emerged. Two approaches to accomplish the analysis of the target of interest are Resistive-Pulse Sensing (RPS) (Sexton et al. 2010) and Ion-Current Rectification (ICR) (Fan et al. 2013; Momotenko and Girault 2011), respectively. For nanopore in thin membrane and engineered protein nanopore, Resistive-Pulse Sensing is an exclusive choice (Sexton et al. 2007). With

respect to the asymmetric nanopore in thick polymer membranes such as polyethylene terephthalate (PET) and polycarbonate (PC) membranes (Yang et al. 2013), both approaches can be used. However, Ion Current Rectification (Gao et al. 2014; Guo et al. 2011b) is much more preferable than Resistive-Pulse Sensing. Firstly, the ion current rectification ratio exhibited by the asymmetric nanopore is highly adjustable, which shows large value even though the tip diameter is up to 50 nm (Wang and Martin 2008). Secondly, the surface area around the nanopore tip plays a very crucial role in the molecular recognition, which increases the capturing efficiency. On the contrary, this feature could degrade the detection efficiency of the sensor based on RPS, since the target could be irreversibly bound to the nanopore surface without dissociation from the surface due to the multivalent binding affinity. In 2008, Wang et al. applied ICR in analysis of positively hydrophobic drugs with conically shaped nanopore in kapton membrane(Wang and Martin 2008). Then other possible applications of the artificial nanopores such as the detection of single molecules (Gao et al. 2014; Wang and Martin 2008; Wen et al. 2013), protein(Ali et al. 2011a; Ali et al. 2013; Ali et al. 2010; Ali et al. 2011b), DNA (Fu et al. 2009), metal ion(Han et al. 2013; Tian et al. 2013) and biomoleculars (Liu et al. 2013; Tian et al. 2010; Zhang et al. 2013) were achieved.

Several factors, including buffer solution, pore size, pore geometry and charge density, can be exploited to modulate the ion current rectification ratio for asymmetric nanopore. For sensing applications, adjusting the surface charge is the most effective way to construct a nanopore-based sensor. In order to make the nanopore sensor highly sensitive and selective, functionalization of the nanopore surface is the most commonly used method. As compared with those robust analytical techniques (Gao et al. 2011; Lin et al. 2011; Lu et al. 2013; Pu et

al. 2012; Song et al. 2014; Wang et al. 2007b; Wang et al. 2012; Zhang et al. 2010; Zhou et al. 2012), the sensitivity and selectivity are far less satisfactory. The obstacle is lack of an efficient way to design the nanopore surface. The ideal sensor platform based on cone-shaped nanopore must feature the property that low concentration of target can reverse the surface charge status significantly after target interacts with the probe-immobilized nanopore surface. But unfortunately, it is not easy to find a probe whose net charge is opposite to the target of interest. Furthermore, probe immobilization brings high steric hindrance and also changes the hydrophobicity of the nanopore, which is not favorable for target binding.

In the present study, a new paradigm based on cone-shaped nanopore combined with SWNTs is proposed. The nanopore coated with Zr^{4+} acts as a counter which can quantitatively detect the concentration of folded DNA (or aptamer); at the same time, SWNTs can remove the excess single-stranded DNA (ssDNA) (or aptamer) which has not folded into duplex conformation the presence of target (Guo et al. 2010; Guo et al. 2011a; Zhang et al. 2010). Zirconium ion (Zr^{4+}) which has strong affinity with the phosphate containing groups, is considered as an ideal candidate for immobilization or detection of biomolecules with phosphate groups (Shervedani and Pourbeyram 2009). Similar studies have demonstrated the adsorption of DNA via phosphate groups (Fang et al. 2011; Liu et al. 2004; Wang et al. 2007b) or the immobilization of laccase via enzyme carboxylate terminal groups onto the solid surface modified by Zr^{4+}(Fang et al. 2008; Fang et al. 2011; Meng et al. 2012; Qi et al. 2013).

By taking ATP detection as an incarnation of this new paradigm, a new sensor for ATP detection is constructed as illustrated in Scheme 1. The presence of ATP induces the folding ATP aptamer into a compact structure with the formation of aptamer-ATP complexes (Wang et

al. 2007b). The SWNTss could facilely remove the unbound aptamer instead of the compact complex. The compactly folded structure has much weaker adsorption propensity than the free aptamer.(Song et al. 2014; Wang et al. 2012). Instead, the aptamer-ATP complexes can be easily accumulated on the nanopore surface via the Zr^{4+}-PO_4^{3-} interaction. Before the DNA adsorption, the nanopore coated with Zr^{4+}-PEI is positively charged. Whereas negatively charged DNA can neutralize the surface charge of the nanopore, leading to the change of current through nanopore which can be monitored by I-V curves. Therefore, the concentration of ATP could be indirectly quantitated and this sensor is also demonstrated to be selective toward ATP instead of other ATP analogues such as UTP, CTP, and GTP).

2. Experimental

2.1. Chemicals and materials

12 μm thick polyethylene terephthalate (PET) which was irradiated with swift Au ion of 11.4 GeV/nucleon at UNILAC linear accelerator to create a single damage track through the membrane were obtained from GSI, Darmstadt, Germany. Potassium chloride (KCl), sodium hydroxide (NaOH) were purchased from Beijing Chemical Reagent Company (Beijing, China). Single-walled carbon nanotubes were purchased from Chengdu Organic Chemicals Co. Ltd. (Chengdu, China). The surfactant DOW fax 2A1 was obtained from DOW Chemical. Tris and zirconium acetate was purchased from aladdin reagent. Polyethyleneimine (M_w=25000, branched PEI), adenosine triphosphate (ATP), guanosine triphosphate (GTP), cytidine triphosphate (CTP) and uridine triphosphate (UTP) were purchased from Sigma–Aldrich. Ultrapage purified oligonucleotides were obtained from Sangon Biotechnology Co.,

Ltd. (Shanghai, China). ATP binding aptamer 5'-ACCT GGGG GAGT ATTG CGGA GGAA GGT-3'. The FAM-labeled ATP aptamer 5'-ACCT GGGG GAGT ATTG CGGA GGAA GGT-FAM-3'. Oligonucleotides were stored at -20 ^{o}C and were heated to 95 ^{o}C for 5 min and gradually cooled to room temperature before use.

2.2 Nanopore preparation

Single conical nanopore was prepared in 12 μm thick polyethylene terephthalate (PET) membrane by the track-etching technique. Either side of the tracked PET membrane was independently exposed to the UV light (365 nm and 254 nm) for 1 h, and then the membrane was embedded between two chambers of a conductivity cell so that different electrolyte solution could be placed on each side of the PET membrane. The procedure of chemical etching included two steps. An etching solution (6 M NaOH) was placed on one side of the membrane and a protecting solution which neutralized the etchant (1 M HCOOH and 0.7% 2A1) was placed on the other at 40 ^{o}C for 1.5 h in the first etching step. Each side of conductivity cell was added with a Pt wire. A Keithley 2536A picoammeter/voltage-source (Keithley Instruments, Cleveland, OH) was employed to measure the ion current while chemical etching using a transmembrane potential of 1 V. In the second step, the membrane was placed in the centrifuge tube containing 2 M NaOH for 5 min at 65 ^{o}C. The same operating procedure was applied to the multi-tracked PET membranes (1×10^{6} tracks cm^{-2}). The tip diameter of the different nanopores was 74 nm, 82 nm, 78 nm, 92nm according to the formula (Figure S2) respectively, while base diameter of the nanopore was 1100 nm (Figure S1).

2.3 Chemical modification of the nanopore

Polyethyleneimine was immobilized onto the PET surface through electrostatic adsorption. Then an aqueous solution of polyethyleneimine (PEI, 1% wt) was placed on both sides of the track-etched membrane for 5 h. After polyethyleneimine was immobilized onto the membrane, an aqueous solution of zirconium acetate (8% wt) was placed on the tip side of the conical nanopore for 30 min. All the reactions were conducted at 25 ^{o}C.

2.4 Field-emission scanning electron microscopy and XPS characterization

The field-emission scanning electron microscopy (ESEM XL-30) was utilized to image the morphology of the nanopores. Multi-tracked PET membranes (1×10^{6} tracks cm^{-2}) was prepared as described in the Experiment 2.2. The images of tip and base side of the nanopore were shown in the Figure S1 (supporting information).

X-ray photoelectron spectroscopy (XPS) was used to characterize the surface chemistry of the multi-tracked PET membranes. XPS data were obtained with an ESCALab250i-XL electron spectrometer from VG Scientific using 300 W Al Kα radiations.

2.5 Current-versus-voltage measurements of nanopore

Ion current was measured by Keithley 2536A picoammeter/voltage-source (Keithley Instruments, Cleveland, OH). The membrane was embedded in a two chambers of a conductivity cell filled with Tris-HCl buffer solution (pH=7.4, 100 mM KCl 10mM Tris). Ag/AgCl electrodes were placed in each side of the conductivity cell to measure a transmembrane potential across the membrane. The transmembrane potential was varied from -1V to 1V.

2.6 Procedure for sensing aptamer

ATP binding aptamer of different concentration was initially added on the tip side of the

conical nanopore. A 5 min voltage scan from -1V to 1V was employed to facilitate accumulation of probe onto the surface of the conical nanopore.

2.7 Procedure for sensing the aptamer-ATP complexes

Different concentrations of ATP from 50 nM to 10 μM were mixed with 1 μM binding aptamer (200 μL) in the centrifuge tube for 2 h. And then, 500 μg/mL single-walled carbon nanotubes (100 μL) was added to the centrifuge tube and wait for another 30 min (Guo et al. 2012). The resulting solution was diluted to 1 mL with Tris-HCl buffer. After that, the mixture was placed on the tip side of the conical nanopore and detected as described above.

2.8 Cellular ATP assay

The Hela cell was cultured in RPMI-1640 medium supplemented with 10% fetal bovine serum (FBS) at 37 ^{o}C and in a humidified air contained 5% $CO_{2.}$ The trypsin was added to the cell solution and the digestion was conducted for 4 min. The cell was collected after trypsin digestion, then washed by Tris-HCl buffer three times and suspended in the Tris-HCl buffer again. Cell lysis (approximately 200,000 cells/mL) was obtained by three times of freeze-thaw cycles. Then the solution was used in the detection of ATP.

3. Results and discussion

Ion current rectification is one of the intriguing characteristics for single conical nanopore with charged surface, which attracts increasing attention in recent years. The mechanism of the current rectification has been sufficiently investigated by Z siwy. In 2008, Wang had first employed this phenomenon to prepare a nanopore sensor to detect hydrophobic drug. Afterwards, a lot of nanopore sensors were constructed and widely applied in the detection of

analyte. Relative to the bare nanopore without modifications in early research, more and more studies concentrated on grafting functional groups on the surface of the nanopore to provide recognition sites for analytes. In this study, we applied asymmetric nanopore sensor coated with zirconium ion, using PEI as adhesive layer, to count ATP-aptamer complex for indirect detection of ATP.

3.1. Characterization of chemically-modified nanopore

The whole fabrication and modification process can be easily monitored via ion-current rectification (Figure 1). A nascent nanopore after chemical etching presents abundant carboxyl groups on the nanopore surface and the corresponding ion-current rectification shows a nonlinear curve in the downward shape (Figure 1, black curve). The nonlinear shape can be fully reversed into an upward shape after absorption of PEI polymer in 1% (w/v) aqueous solution for 5 h, indicating the positively-charged status of the nanopore (Figure 1, red curve). Electrostatic interaction between the negative charge on the nanopore surface and the positive charge on the PEI polymer plays a very important role in the adsorption of PEI onto the nanopore surface. Zr^{4+} was confirmed to be easily adsorbed onto the amino-rich PEI polymer by the ion current rectification (Figure 1, blue curve). Until now, few studies have investigated the interaction between Zr^{4+} and PEI, while other metal ions such as Cu^{2+}, Cd^{2+}, Cr^{3+} and Pb^{2+} have been extensively studied in terms of the interaction with PEI (Chen et al. 2010; Fan et al. 2013; Gao et al. 2014; Liu and Huang 2011; McNeff and Carr 1995).

With only PEI coated, the nanopore shows negligible response to phosphate-rich DNA polymer with 27 bases, which is clearly demonstrated in Figure 2A. It can be concluded that the electrostatic interaction between short DNA and positively charged PEI is not strong

enough to allow the current change via the nanopore. In contrary to PEI-coated nanopore, the nanopore coated with PEI/Zr^{4+} shows DNA concentration-dependent current responses (Figure 2B). The strong interaction between Zr^{4+} and phosphoric group plays very important roles, which has already been manifested in many studies (Shervedani and Pourbeyram 2010; Wang et al. 2007a). For sensing purpose, the surface adsorption of free DNA is extremely unfavorable for achievement of the sensor quality. In order to resolve this issue, SWNTs which have been proved to bind single strand DNA are added into the DNA solution. Figure 2C clearly shows that the free DNA adsorption can be efficiently prevented. The ratio of SWNTs to the ATP aptamer was systematically investigated (Figure S5). The 50 μg/mL concentration of SWNTs was chosen in the presence of 200 nM aptamer. Finally, whether free ATP as a biomolecule with phosphate groups could contaminate the nanopore surface was investigated (Figure 2D), it obviously shows that the ATP concentrations up to 10 μM only had negligible influence on the ion-current rectification.

Fig. 1

Fig. 2

3.3 Optimization of the SWNTs concentration

The ratio of the SWNTs concentration to aptamer is pretty important since improper ratio could degrade the sensor's sensitivity. The determination of proper ratio was achieved via fluorescence titration. As shown in Fig. S5A (supporting information), with the increasing concentration of the SWNTs, the fluorescence intensity of FAM-labelled DNA was gradually decreased since the aptamer was adsorbed onto the surface of SWNTs. At a concentration of 50 μg/mL SWNTs, more than 95% FAM's fluorescence was quenched. So 50 μg/mL SWNTs

was adopted in the presence of 200 nM aptamer for the subsequent experiments. All the nanopore tests (Figure 2D) showed that this concentration was sufficient enough to eliminate the interference of free aptamer. The detailed structure of SWNTs measured by Transmission Electron Microscopy (TEM) is shown in Figure S3 (Supporting Information)

3.4 Confirmation of Zr^{4+} coating by XPS characterization

X-ray photoelectron spectroscopy (XPS) was used to characterize the surface chemistry of the multi-tracked PET membranes. XPS data were obtained with an ESCALab250i-XL electron spectrometer from VG Scientific using 300 W Al Kα radiations. Fig. S4A (Supporting information) clearly shows a much higher value of the N_{1s} peak in XPS spectra for the PET membrane after PEI adsorption compared to the naked PET membrane. PEI adsorption provided tons of anchoring points for the subsequent metal ion coating. Since a number of literatures (Shervedani and Pourbeyram 2010; Wang et al. 2007a) have reported that Zr^{4+} strongly binds DNA via electrostatic force, polyvalent Zr^{4+} was applied in our experiments. The XPS spectra (Figure S4B) demonstrate that Zr^{4+} was successfully coated onto the PEI adsorbed on track-etched membrane. The peaks corresponding to Zr (3d3/2 at 181.85 eV; 3d5/2 at 183.75 eV) are only observable in Figure S4B (b) after Zr^{4+} coating, while there is no peaks for the PET surface without any modification as shown in Figure S4B (a).

3.5 Quantitative Detection of ATP

The concentration of ATP determines the complex (ATP/aptamer) concentration, which can be monitored by the I-Vcurve. With the fixation of aptamer and SWNTs concentration at 200 nM and 50 μg/L, respectively, the concentration of the complex (ATP/Aptamer) in

solution has linear relationship with the ATP concentration in solution. Therefore, the ATP concentration can be indirectly quantitated by asymmetrical nanopore coated with PEI/Zr^{4+}. The adsorption behavior of the complex (ATP/Aptamer) adheres to Langmuir absorption model. The ATP concentration was indirectly monitored by the change of the I-Vcurve after the adsorption of the complex onto the nanopore surface. According to the Langmuir model reported previously (Wang and Martin 2008), the surface coverage (θ) is related with the ATP concentration via the equation 1.

$$\theta = KC/(1+KC) \quad (1)$$

Where θ is the fractional coverage of the molecule on the surface, K is the binding constant and C is the concentration of the ATP. θ is also given by

$$\theta = (I_0 - I_i)/(I_0 - I_{min}) \quad (2)$$

Where I_0 is the current through the nanopore in the absence of the ATP, I_{min} is the minimum current after the nanopore surface is saturated by high concentrated ATP. And I_i is defined as the corresponding ion current exposed to the solution which is the immediate concentration of ATP. The surface coverage (θ) plotted as the function of ATP concentration shows linear relationship with ATP concentration below 200 nM (Figure 3). The limit of detection (LOD) is calculated to be 27.46 nM according to the equation LOD = 3N/S.

Scheme 1

Fig. 3

3.7 Selectivity of the nanopore sensor toward ATP

The selectivity tests of the biosensor were conducted by examining the nanopore responses to the ATP over the analogues of ATP such as CTP, UTP, GTP. 1 μM concentration

for the ATP and analogues were chosen. Under the same experimental conditions, the I-V curve was acquired (Figure 4A). It was manifested in Figure 4B that the rectification ratio in presence of ATP was changed much larger than that in presence of CTP, UTP and GTP since those three analogues could not interact with the aptamer. The results demonstrated the remarkable selectivity of the biosensor for the ATP is attributed to the specific interaction between ATP and aptamer.

Fig. 4

3.8 Analysis of ATP in Hela cell

In order to prove this method can be used in the real samples, the biosensor was employed to detect ATP from hela cell. Since the freezing and thawing technique allowed the cellular content to flow out after cellular membrane disruption, ATP measured by nanopore can be an indication of the ATP content in the cancer cell. As shown in Figue 5A and 5B, ATP content measured immediately after cell membrane disruption by freezing and thawing technique was distinctly higher than that measured 24 hours later after cell membrane disruption. These experimental results were consistent with many other studies reported previously (Zhang et al. 2010). Undoubtedly, this sensing platform possesses the ability to analyze the real sample.

Fig. 5

3.9 The regeneracy of the synthetic nanopore sensor

Reusability of synthetic nanopore is an very important criteria to evaluate the quality of the sensor. Until now, the progress in this aspect is still in a very early stage. Herein we challenged our nanopore sensor by regenerating the nanopore surface for several times. The I-V curve in Figure S6A shows that short time etching with 2M NaOH for 5 minutes was

good enough to remove the aptamer from the surface. Recycling the nanopore sensor for up to 4 times has been implemented (Figure S6B). As we know, longer etching can enlarge the nanopore size significantly, therefore, long-term recycling of nanopore sensor is not recommended.

4. Conclusions

In this study, we developed a label-free nanopore biosensor for the detection of ATP in conjunction with SWNTs. This simple method evades direct immobilization of probe molecules onto the asymmetric nanopore surface, whereas both selectivity and sensitivity can be warranted. The key point of this strategy lies in that any aptamer-binding target can be quantitated by counting the DNA concentration via the Zr^{4+}-coated nanopore sensor and free interfering DNAs can be drawn away by SWNTs. The detection limit of this nanopore sensor for ATP is 27.46 nM. Although only detection of ATP is demonstrated in this study, this scenario can be expanded to analyze other target since there are a lot of studies regarding the interaction between aptamer and other molecules. In the future research, signal amplification will be integrated into this system for further improvement of sensitivity and selectivity.

Acknowledgements

This work was supported by National Natural Science Foundation of China (No. 21190040 and 21275137), Start Funding from Changchun Institute of Applied Chemistry (CAS) and Supporting Funding for Creative Young Scientist (CAS). Thanks for GSI providing track-etched membranes.

References

Ali, M., Nasir, S., Nguyen, Q.H., Sahoo, J.K., Tahir, M.N., Tremel, W., Ensinger, W., 2011a. Journal of the American Chemical Society 133(43), 17307-17314.
Ali, M., Nasir, S., Ramirez, P., Cervera, J., Mafe, S., Ensinger, W., 2013. The Journal of Physical Chemistry C 117(35), 18234-18242.
Ali, M., Nguyen, Q.H., Neumann, R., Ensinger, W., 2010. Chemical Communication 46(36), 6690-6692.
Ali, M., Ramirez, P., Tahir, M.N., Mafe, S., Siwy, Z., Neumann, R., Tremel, W., Ensinger, W., 2011b. Nanoscale 3(4), 1894-1903.
Chen, Y., Pan, B., Li, H., Zhang, W., Lv, L., Wu, J., 2010. Environmental Science & Technology 44(9), 3508-3513.
Fan, H.-T., Liu, J.-X., Sui, D.-P., Yao, H., Yan, F., Sun, T., 2013. Journal of Hazardous Materials 260, 762-769.
Fang, C., Agarwal, A., Buddharaju, K.D., Khalid, N.M., Salim, S.M., Widjaja, E., Garland, M.V., Balasubramanian, N., Kwong, D.L., 2008. Biosensors & bioelectronics 24(2), 216-221.
Fang, C., Ji, H., Karen, W.Y., Rafei, S.R., 2011. Biosensors & bioelectronics 26(5), 2670-2674.
Fu, Y., Tokuhisa, H., Baker, L.A., 2009. Chemical Communication (32), 4877-4879.
Gao, H., Xi, M., Xu, L., Sun, W., 2011. Microchimica Acta 174(1-2), 115-122.
Gao, J., Sun, S.-P., Zhu, W.-P., Chung, T.-S., 2014. Journal of Membrane Science 452, 300-310.
Guo, W., Xia, H., Cao, L., Xia, F., Wang, S., Zhang, G., Song, Y., Wang, Y., Jiang, L., Zhu, D., 2010. Advanced Functional Materials 20(20), 3561-3567.
Guo, Z., Ren, J., Wang, J., Wang, E., 2011a. Talanta 85(5), 2517-2521.
Guo, Z., Wang, J., Ren, J., Wang, E., 2011b. Nanoscale 3(9), 3767-3773.
Guo, Z., Wang, J., Wang, E., 2012. Talanta 89, 253-257.
Han, C., Su, H., Sun, Z., Wen, L., Tian, D., Xu, K., Hu, J., Wang, A., Li, H., Jiang, L., 2013. Chemistry A European Journal 19(28), 9388-9395.
Lin, Z., Luo, F., Liu, Q., Chen, L., Qiu, B., Cai, Z., Chen, G., 2011. Chemical Communication 47(28), 8064-8066.
Liu, B., Huang, Y.M., 2011. Polyethyleneimine modified eggshell membrane as a novel biosorbent for adsorption and detoxification of Cr(VI) from water. J. Mater. Chem. 21(43), 17413-17418.
Liu, N., Jiang, Y., Zhou, Y., Xia, F., Guo, W., Jiang, L., 2013. Angew Chem Int Ed Engl 52(7), 2007-2011.
Liu, S., Dong, Y., Zhao, W., Xie, X., Ji, T., Yin, X., Liu, Y., Liang, Z., Momotenko, D., Liang, D., Girault, H.H., Shao, Y., 2012. Analytical chemistry 84(13), 5565-5573.
Liu, S.Q., Xu, J.J., Chen, H.Y., 2004. Colloids Surf B Biointerfaces 36(3-4), 155-159.
Lu, J., Yan, M., Ge, L., Ge, S., Wang, S., Yan, J., Yu, J., 2013. Biosensors & bioelectronics 47, 271-277.
McNeff, C., Carr, P.W., 1995. Anal Chem 67(21), 3886-3892.
Meng, H.M., Fu, T., Zhang, X.B., Wang, N.N., Tan, W., Shen, G.L., Yu, R.Q., 2012. Analytical chemistry 84(5), 2124-2128.
Momotenko, D., Girault, H.H., 2011. Journal of the American Chemical Society 133(37), 14496-14499.

Pu, W.D., Zhang, L., Huang, C.Z., 2012. Analytical Methods 4(6), 1662-1666.
Qi, W., Zhao, J., Zhang, W., Liu, Z., Xu, M., Anjum, S., Majeed, S., Xu, G., 2013. Analytica chimica acta 787, 126-131.
Sexton, L.T., Horne, L.P., Sherrill, S.A., Bishop, G.W., Baker, L.A., Martin, C.R., 2007. Journal of the American Chemical Society 129(43), 13144-13152.
Sexton, L.T., Mukaibo, H., Katira, P., Hess, H., Sherrill, S.A., Horne, L.P., Martin, C.R., 2010. Journal of the American Chemical Society 132(19), 6755-6763.
Shervedani, R.K., Pourbeyram, S., 2009. Biosensors & bioelectronics 24(7), 2199-2204.
Shervedani, R.K., Pourbeyram, S., 2010. Bioelectrochemistry 77(2), 100-105.
Song, Y., Yang, X., Li, Z., Zhao, Y., Fan, A., 2014. Biosensors & bioelectronics 51, 232-237.
Tian, Y., Hou, X., Wen, L., Guo, W., Song, Y., Sun, H., Wang, Y., Jiang, L., Zhu, D., 2010. Chemical Communication 46(10), 1682-1684.
Tian, Y., Zhang, Z., Wen, L., Ma, J., Zhang, Y., Liu, W., Zhai, J., Jiang, L., 2013. Chem Commun 49(91), 10679-10681.
Wang, J., Martin, C.R., 2008. Nanomedicine 3(1), 13-20.
Wang, J., Wang, F., Xu, Z., Wang, Y., Dong, S., 2007a. Talanta 74(1), 104-109.
Wang, J., Wang, L., Liu, X., Liang, Z., Song, S., Li, W., Li, G., Fan, C., 2007b. Advanced Materials 19(22), 3943-3946.
Wang, L., Zhu, J., Han, L., Jin, L., Zhu, C., Wang, E., Dong, S., 2012. Acs Nano 6(8), 6659-6666.
Wen, L., Sun, Z., Han, C., Imene, B., Tian, D., Li, H., Jiang, L., 2013. Chemistry A European Journal 19(24), 7686-7690.
Yang, L., Zhai, Q., Li, G., Jiang, H., Han, L., Wang, J., Wang, E., 2013. Chemical Communication 49(97), 11415-11417.
Zhang, H., Tian, Y., Jiang, L., 2013. Chemical Communication 49(86), 10048-10063.
Zhang, L., Wei, H., Li, J., Li, T., Li, D., Li, Y., Wang, E., 2010. Biosensors & bioelectronics 25(8), 1897-1901.
Zhou, Z.M., Yu, Y., Zhao, Y.D., 2012. The Analyst 137(18), 4262-4266.

Figure captions.

Scheme 1. Schematic of the biomimetic nanopore preparation and the detection of ATP. (a) A cone-shaped nanopore with abundant carboxyl groups on the surface. (b) Electrostatic adsorption of PEI onto the nanopore. (c) Adsorption of Zr^{4+} onto the PEI-coated nanopore. (d) Detection of aptamer-ATP complexes via the nanopore. The SWNTs remove the excess ssDNA.

Fig. 1. I-V curve characterization of each preparation step of the biomimetic nanopore (tip diameter = 92 nm, base diameter = 1100 nm). Nascent nanopore with abundant carboxyl groups (black square), nanopore coated with PEI (red circle), nanopore coated with PEI/Zr^{4+} (blue triangle).

Fig. 2. (A) The responses of PEI-coated asymmetric nanopore (tip diameter = 92 nm, base diameter = 1100 nm) to various concentrations of aptamer. (B) The responses of PEI/Zr^{4+}-coated asymmetric nanopore (tip diameter = 74 nm, base diameter = 1100 nm) to various concentrations of aptamer. (C) The responses of PEI/Zr^{4+}-coated asymmetric nanopore (tip diameter = 78 nm, base diameter = 1100 nm) to 200 nM aptamer in the presence of 50 μg/mL SWNTs. (D) The responses of PEI/Zr^{4+}-coated asymmetric nanopore (tip diameter = 78 nm, base diameter = 1100 nm) to various concentrations of ATP.

Fig. 3. (A) The ATP concentration-dependent responses of PEI/Zr^{4+}-coated asymmetric nanopore (tip diameter = 78 nm, base diameter = 1100 nm) in the presence of 200 nM aptamer and 50 μg/mL SWNTs. (B) Plot of surface coverage (θ) versus ATP concentration. Red line is the fitting curve based on langmuir model. The inset displays the linear response for ATP concentration ranging from 0 nM to 200 nM.

Fig. 4. Selectivity of PEI/Zr^{4+}-coated asymmetric nanopore (tip diameter = 78 nm, base diameter = 1100 nm) toward ATP against other ATP analogue. (A) The responses of asymmetric nanopore sensor to UTP (1 μM), GTP (1 μM), CTP (1 μM) and ATP (1 μM), respectively, in the presence of 200 nM aptamer and 50 μg/mL SWNTs. (B) The corresponding columns whose values are the relative ratio of current change measured at +1 V.

Fig. 5. (A)The response of asymmetric nanopore sensor (tip diameter = 82 nm, base diameter = 1100 nm) to ATP in Hela cell. (a) Only buffer solution, (b) buffering solution plus 200 nM aptamer and 50 μg/mL SWNTs, (c) in the presence of lysed cells after 24-h aging (ATP absent) under otherwise same conditions as (b), (d) in the presence of freshly lysed cells (ATP present) under otherwise same conditions as (b). (B) The corresponding columns whose values are the relative ratio of current change measured at +1 V.

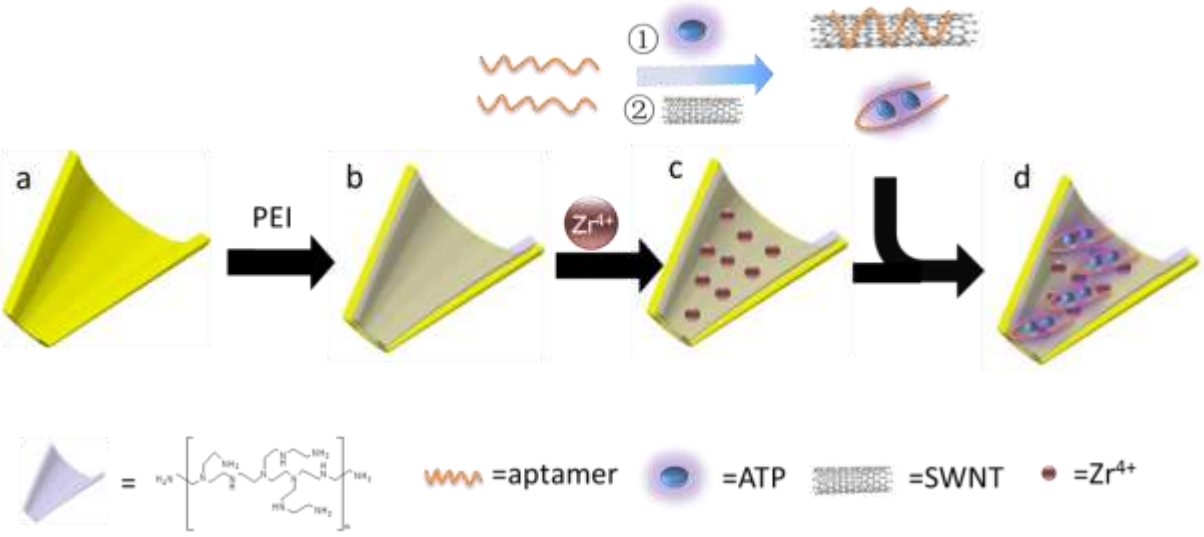

Scheme 1.

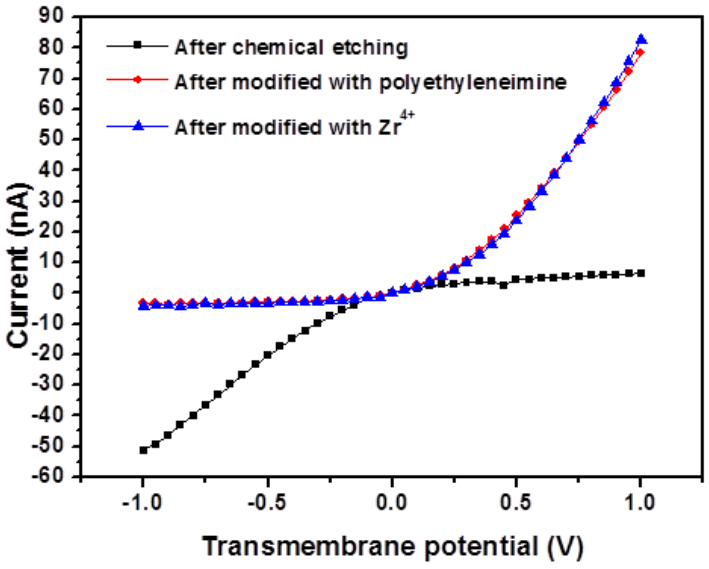
After chemical etching
After modified with polyethyleneimine
After modified with Zr4+
Current (nA)
Transmembrane potential (V)
90
80
70
60
50
40
30
20
10
0
-10
-20
-30
-40
-50
-60
-1.0
-0.5
0.0
0.5
1.0

Fig. 1.

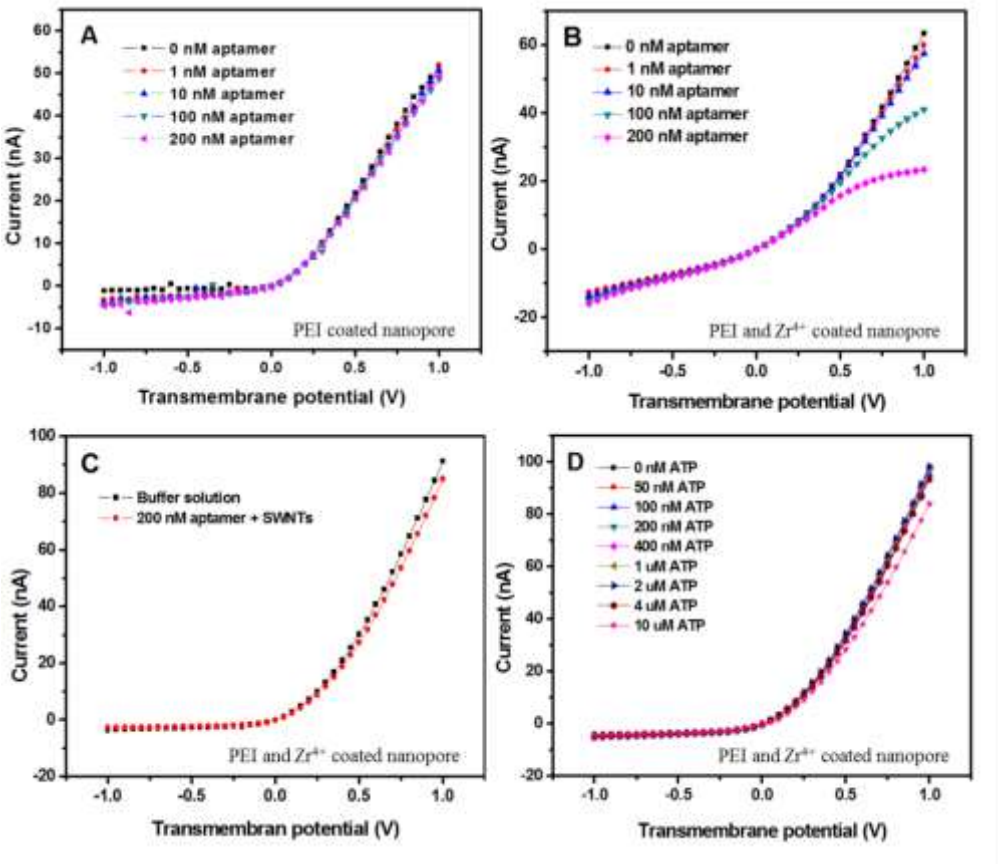
A
0 nM aptamer
1 nM aptamer
10 nM aptamer
100 nM aptamer
200 nM aptamer
PEI coated nanopore
Current (nA)
Transmembrane potential (V)
B
0 nM aptamer
1 nM aptamer
10 nM aptamer
100 nM aptamer
200 nM aptamer
PEI and Zr4+ coated nanopore
Current (nA)
Transmembrane potential (V)
C
Buffer solution
200 nM aptamer + SWNTs
PEI and Zr4+ coated nanopore
Current (nA)
Transmembran potential (V)
D
0 nM ATP
50 nM ATP
100 nM ATP
200 nM ATP
400 nM ATP
1 uM ATP
2 uM ATP
4 uM ATP
10 uM ATP
PEI and Zr4+ coated nanopore
Current (nA)
Transmembrane potential (V)

Fig. 2.

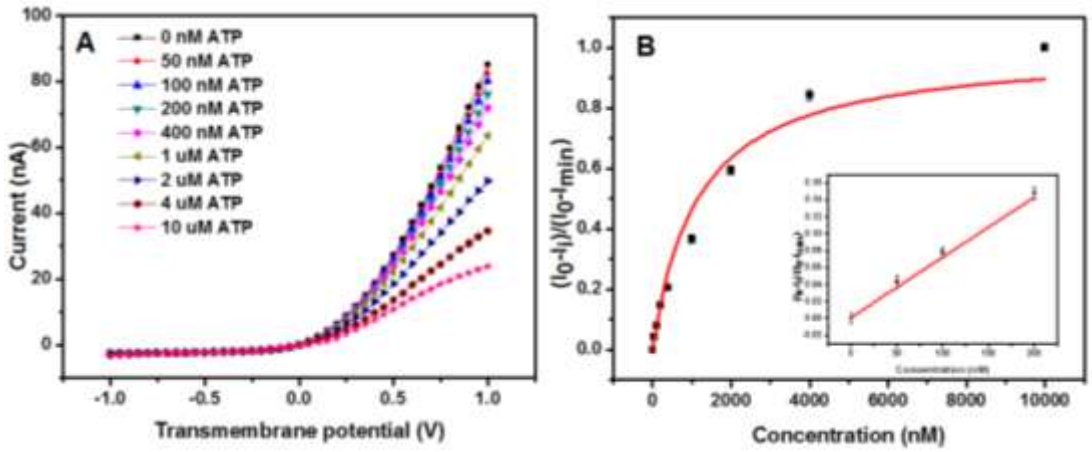
A
0 nM ATP
50 nM ATP
100 nM ATP
200 nM ATP
400 nM ATP
1 uM ATP
2 uM ATP
4 uM ATP
10 uM ATP
Current (nA)
Transmembrane potential (V)
B
Concentration (nM)

Fig. 3.

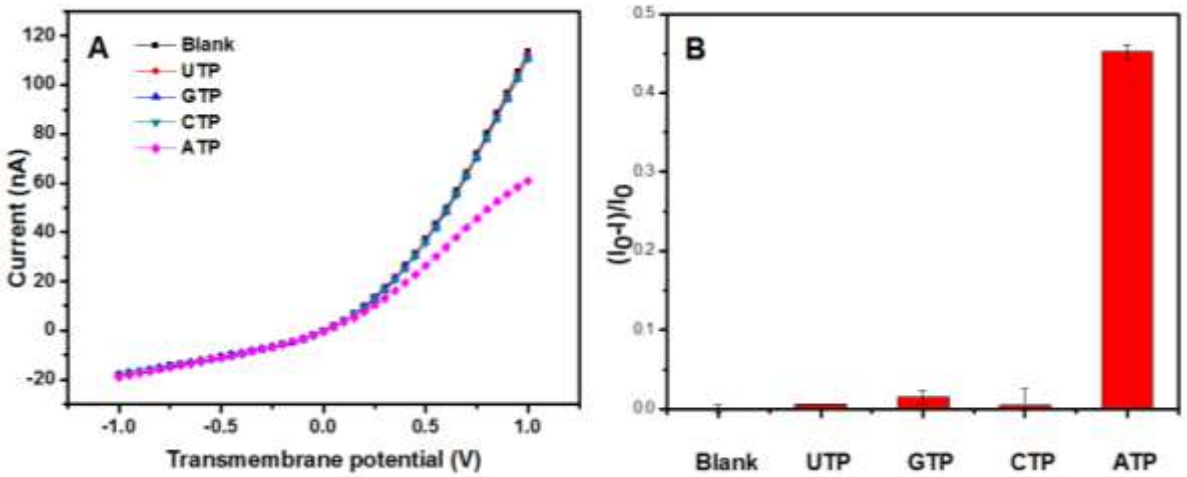
A
Blank
UTP
GTP
CTP
ATP
Current (nA)
Transmembrane potential (V)
B
$(I_0-I)/I_0$
Blank
UTP
GTP
CTP
ATP

Fig. 4.

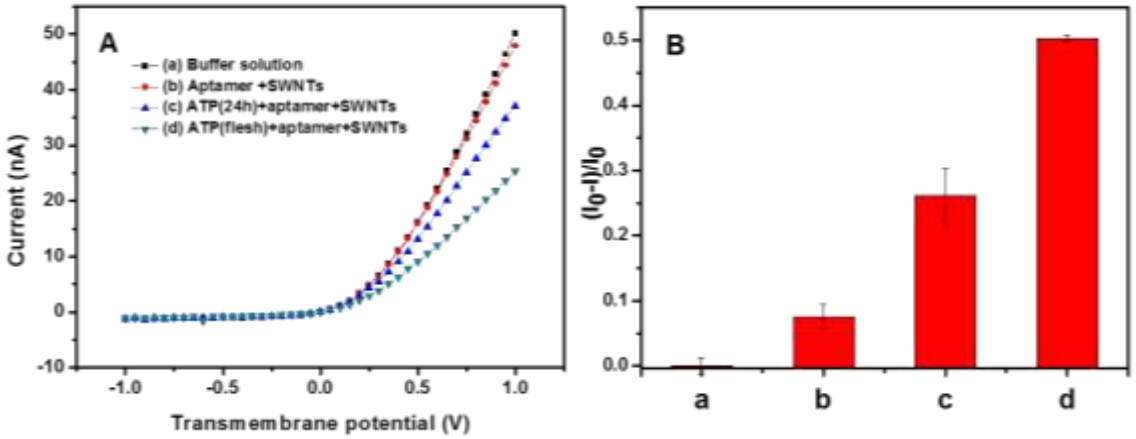
A
(a) Buffer solution
(b) Aptamer +SWNTs
(c) ATP(24h)+aptamer+SWNTs
(d) ATP(flesh)+aptamer+SWNTs
Current (nA)
Transmembrane potential (V)
B
$(I_0-I)/I_0$
a
b
c
d

Fig. 5.

TOC

Without the interference from free target-specific probes that can be eliminated by SWNTs, PET/Zr^{4+} coated nanopore that is responsive to the ATP-bound aptamer can quantitatively detect ATP concentration. In contrast to previous studies based on nanopore, this study evades the immobilization of target-specific probe onto the nanopore surface.